Random population model to explain the recombination dynamics in single InAs/GaAs quantum dots under selective optical pumping

2011 New J. Phys. 13 023022

(http://iopscience.iop.org/1367-2630/13/2/023022)

New Journal of Physics
The open-access journal for physics

Random population model to explain the recombination dynamics in single InAs/GaAs quantum dots under selective optical pumping

Jordi Gomis-Bresco[1,4,5], Guillermo Muñoz-Matutano[1], Juan Martínez-Pastor[1], Benito Alén[2], Luca Seravalli[3], Paola Frigeri[3], Giovanna Trevisi[3] and Secondo Franchi[3]

[1] Institut de Ciències dels Materials de la Universitat de València, Universitat de València, València, Spain
[2] IMM, Instituto de Microelectrónica de Madrid (CNM, CSIC), Isaac Newton 8, 28760 Tres Cantos, Madrid, Spain
[3] CNR-IMEM Institute, Parco delle Scienze 37a, I-43100 Parma, Italy
E-mail: jrdi.gomis@icn.cat

New Journal of Physics **13** (2011) 023022 (17pp)
Received 25 July 2010
Published 9 February 2011
Online at http://www.njp.org/
doi:10.1088/1367-2630/13/2/023022

Abstract. We model the time-resolved and time-integrated photoluminescence of a single InAs/GaAs quantum dot (QD) using a random population description. We reproduce the joint power dependence of the single QD exciton complexes (neutral exciton, neutral biexciton and charged trions). We use the model to investigate the selective optical pumping phenomenon, a predominance of the negative trion observed when the optical excitation is resonant to a non-intentional impurity level. Our experiments and simulations determine that the negative charge confined in the QD after exciting resonance to the impurity level escapes in 10 ns.

[4] Present address: Catalan Institute of Nanotechnology CIN2(ICN-CSIC), Campus de la UAB, 08193 Bellaterra, Barcelona, Spain.
[5] Author to whom any correspondence should be addressed.

Contents

1. Introduction

Owing to its zero-dimensional nature, the photoluminescence of a single InAs/GaAs quantum dot (QD) presents sharp spectral lines, corresponding to radiative recombination of an electron–hole pair or exciton. Depending on the number of electrons and holes confined in the QD, the energy of emission shifts due to Coulomb correlations. These effects produce a typical spectrum of several lines attributed to excitons, biexcitons and positive and negative trions emitted by the same single QD [1]. Their temporal dynamics can be measured by separately filtering the wavelength of emission and time resolving the isolated complexes. But as they belong to a common emitter, they have to be modelled accordingly. With that goal in mind, we use a random population model (RPM) to describe the stationary and time resolved emission of a single QD with only s shell electron and hole levels confined. The RPM [2] was developed to describe the dynamics of QD ensembles. In contrast to rate equations, we count the probability of finding the QD in a particular charge configuration, called the microstate, instead of the average occupation of the confined levels. The power dependence of the excitonic complexes (neutral exciton, neutral biexciton and trions) appears naturally as a solution of the RPM, as we will show below. Abbarchi *et al* [3] show that, when limiting the model to take into account only excitonic levels and continuous wave stationary excitation, the power dependence of the excitonic complexes precisely follows Poissonian statistics, capable of reproducing the experimental power dependence of the complexes emitted by a single QD. In particular, we use the RPM to investigate the selective optical pumping phenomenon, a predominance of the negative trion observed when the optical excitation is resonant with a non-intentional impurity level. An excess of electrons is optically generated in the vicinity of the QD and effectively captured into it [4, 5]. A better control of the exact charge at the QD could be achieved by using selective optical pumping with an extra infrared excitation below the energy level of the QD ground state energy [6]. We measured, at cryogenic temperature ($T = 10\,\mathrm{K}$), time-resolved and time-integrated photoluminescence of a single InAs/GaAs QD that shows selective optical pumping. We chose two exemplary excitations: excitation in the GaAs barrier (no excess of

electrons generated) and resonant to the non-intentional impurity level (excess of electrons captured in the QD). We fitted the experimental measurements with the RPM and determined that the negative charge confined in the QD, after exciting resonance to the impurity level, escapes in 10 ns. The paper is divided into six sections. We describe the sample and the experiment in section 2. Afterwards, we present our experimental results. In section 4, we introduce the RPM and adapt it to account for our experimental observations. In section 5, we simulate our experiments and discuss the results. Finally, we present our conclusions in the last section.

2. The sample and experiments

We study the Stransky–Krastanov InAs/GaAs QDs grown by molecular beam epitaxy. The combination of low growth rate and graded coverage allows us to obtain very-low-density samples [7], which are suitable for single QD spectroscopy and represent a possible basis for single/entangled photon sources. The sample under study has a density of 16.5 QDs per μm^2, as estimated by atomic force microscopy images. We used a fiber-based confocal microscope to study the single QD spectra. In the confocal microscope spot, we find a small number of QDs, and due to their spectral dispersion, we can perfectly isolate the excitonic emission of a single QD.

Macro- and microphotoluminescence (μPL) experiments as a function of excitation density confirm the existence of only one confined exciton shell. We label the excitonic lines using the most common observation related to the power dependence of the different emission lines, on over ten different QDs examined through different experiments [8, 9]. The energetic splittings measured in our QD agree with what is reported for In(Ga)As shallow single QD [10, 11] even if some dispersion is found depending on size and composition, inherent to real QDs. At high levels of excitation some extra peaks appear, which are attributed to higher charged particles, probably XX configuration with negative/positive extra charges. The identification of X, XX and charged excitons can also be made by using polarization-resolved μPL: both X and XX consist of linearly polarized doublets split by the fine structure splitting (FSS) [12, 13], while X^+ and X^- consist of a single unpolarized line. We have corroborated our preliminary assignation based on the emission line intensity by measuring the FSS in several QDs, whose value is about 40 μeV.

Selective optical pumping is clearly observed in our sample, as we reported in [8, 9]. Hall measurements of similarly grown GaAs buffer layers reveal a residual electron-doping concentration $n = N_{\text{donors}} - N_{\text{acceptors}} \sim 10^{15}\,\text{cm}^{-3}$. This residual impurity concentration is not important in usual samples with higher dot densities, but it will play an important role in low-density samples, as discussed in the next section. Strong differences in the μPL emission are detected as the excitation energy is shifted from non-resonant to resonant with the energy levels of unintentional impurities ($\lambda_{\text{excitation}} = 830\,\text{nm}$). Changes in the emission ratio between the excitonic complexes by varying the excitation wavelength are also observed [8, 14]. This situation is possible due to the promotion of electrons from ionized acceptors to the conduction band. When the excitation energy is above the GaAs barrier ($\lambda_{\text{excitation}} = 775\,\text{nm}$), we observe a smaller contribution of charged excitons. We attribute their appearance to uncorrelated capture of electrons and holes in the QD. Once a photon is generated in the GaAs barrier, the different diffusion of electrons and holes (that have really different mobilities [14]) and their interaction with the QD environment allows unpaired capture.

Using a fast photodiode and a photon-counting card, we can measure micro time-resolved photoluminescence (μTRPL) transients [15, 16], by using a 76 MHz Ti:sapphire laser for

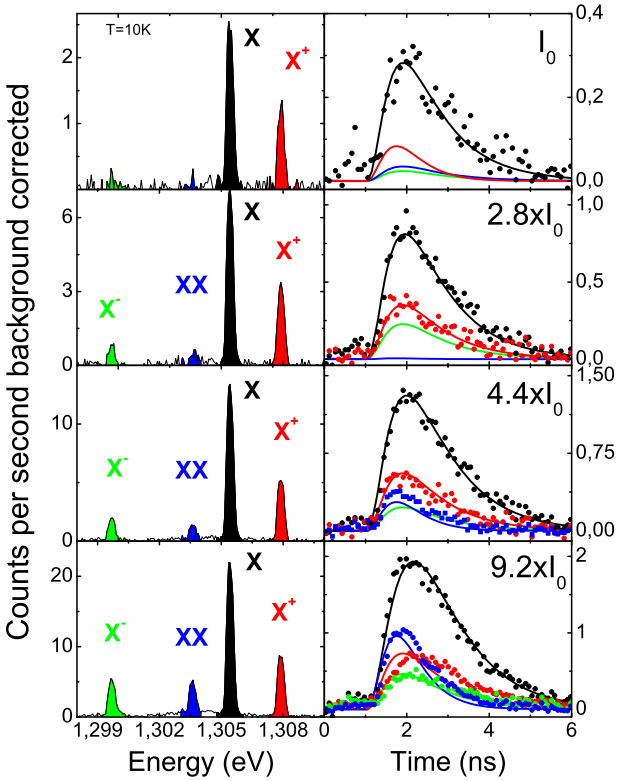

Figure 1. μPL spectra under pulsed excitation conditions and μTRPL transients of a single QD using optical pumping at 775 nm, excitation above the GaAs barrier. Colors in the left panels identify the excitonic complexes and their corresponding μTRPL transients (colored dots) in the right panels. Thin continuous lines (also with colors identifying the excitonic complexes) in time-resolved experiments correspond to the outcome of the microstate model with fitting values given in table 2, as explained below.

experiments exciting at 775 nm (excitation in the GaAs barrier) and a 40 MHz pulsed diode laser when exciting at 830 nm (energy resonant to the levels of unintentional impurities).

3. Experimental results

In figure 1, we show a power dependence μPL and μTRPL evolution from a single QD. μPLs are measured exciting the GaAs barrier ($\lambda_{\text{excitation}} = 775$ nm) with a pulsed source, so μTRPL transients can be directly compared with their corresponding μPL spectra registered under exactly the same excitation conditions. As aforementioned, the energy splittings ($\Delta E_{\text{X-XX}} = 1.6$ meV, $\Delta E_{\text{X-X}^+} = 2.7$ meV, $\Delta E_{\text{X-X}^-} = 5.6$ meV) and the overall structure of the emission resemble the case presented in [8, 9], and excitonic complexes are labeled accordingly. The relative importance of X^+ and X^- varies from QD to QD, a clear hint that the capture of unbalanced charges depends on the interaction of the QD with the near environment and, as a consequence, is a phenomenon that can change locally. In the right-hand side of figure 1, some μTRPL transients are shown (a peak of the μPL spectrum has lost its corresponding μTRPL transient due to signal comparable/below the noise level).

A first exponential fitting of the different excitonic complexes (neutral excitons and positive and negative trions) provides a decay time (τ_r) value around 1.27 ns. The rise times are well below the experimental resolution until the largest excitation power. The biexciton decay time is found to be half of the excitonic lifetime (0.65 ns), reinforcing the labeling of X and XX lines made before. Rise times increase with power, providing reliable fitting values (above 100 ps) only for relatively high powers, when all four complexes are present. The competition between excitonic complexes determines the long values for their rise times. As an extreme example, while biexciton exists and dominates the QD emission the exciton recombination cannot take place, which is translated into an important increase of the μTRPL rise time detected at the X wavelength. This is the situation depicted in the bottom panel of figure 1. To measure excitonic capture times, really low-power excitation is needed; in this case only exciton emission should appear and the rise time extracted through a multiple exponential expression would be approximately the exciton capture time. Nevertheless, the real exciton capture time is well below the time resolution of our setup (100 ps).

Figure 2 shows μPL and μTRPL of the same QD as in figure 1 under pulsed resonant excitation to the impurities level ($\lambda_{excitation} = 830$ nm). This introduces significant differences in the importance of charged excitons with respect to the neutral one, which was attributed to the promotion of electrons from ionized acceptors to ionized donors and conduction band [8, 9]. In the left-hand side of figure 2, it can be observed that the intensity of the previously identified peaks suffers a dramatic change. Now the negative charged exciton dominates the emission spectra at moderate and high excitation powers, while the exciton peak is still the most intense line at the lowest power.

Right panels in figure 2 correspond to the μTRPL transients of the different excitonic peaks in the left panels. The neutral exciton recombination takes place before that of the negative trion (TRPL maximum intensity); at least for the lowest excitation powers (I_0 and $2 \times I_0$), even if the X^- line ends dominating the temporal emission after some ns. The injection of an electron excess in the QD under resonant excitation with the impurity level is slower than the direct capture: an outstanding delay around 300–400 ps is observed (it is clearer for lower excitation power, where there is no 'competition' among the excitonic complexes to hide the capture delay).

We can deduce that the extra electron escapes out of the QD faster than 25 ns (repetition period of the laser): our μTRPL transients are taken under pulsed and periodic excitation (40 MHz pulsed diode laser). The μTRPL transient is not the result of one isolated event but the statistical result of a huge number of events, each of them responding to a particular QD situation; but all events are preceded by a previous excitation. After the negative trion recombination, an unpaired electron remains in the QD. If this electron stays in the QD until the next excitation, the capture of an exciton would lead to another emission of a trion at the beginning of the transients and the emission of the neutral exciton would become impossible, contrary to what we observe. A capture of an extra h^+, several nanoseconds after the excitation, would produce an X emission, but again, we do not observe any long-term X μTRPL tail.

Figure 3 shows the experimental evolution of the PL integrated intensity (IPL) for CW and pulsed excitations resonant with the impurities level ($\lambda_{excitation} = 830$ nm). The most striking observation is the complete change in the X/X^- ratio; while in CW excitation the X^- dominates the emission with a marginal contribution of the X line at high powers, in pulsed excitation the X line dominates the emission at low–medium powers.

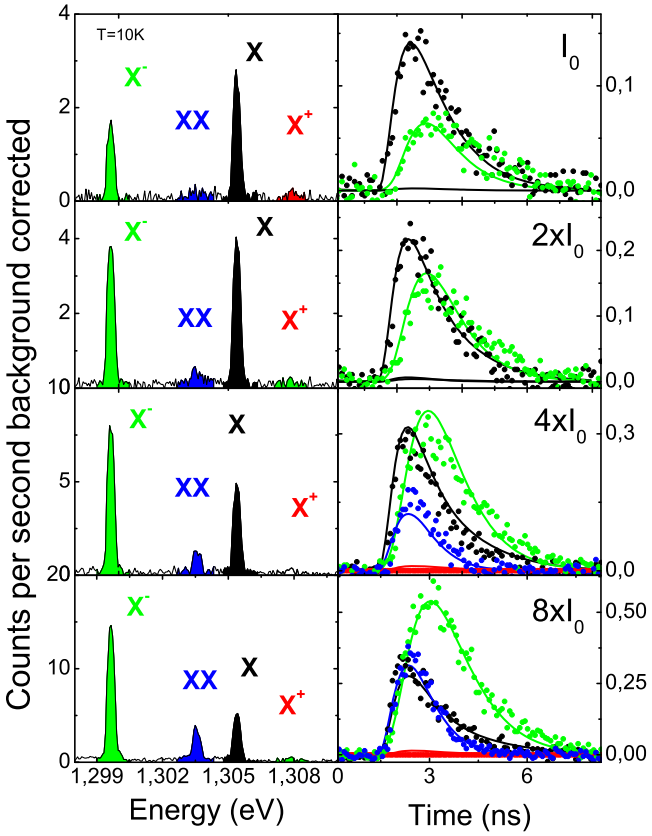

Figure 2. μPL spectra under pulsed excitation conditions and μTRPL transients of a single QD using optical pumping at 830 nm, resonant with the impurities level. Colors in the left panels identify the excitonic complexes and their corresponding μTRPL transients (colored dots) in the right panels. Thin continuous lines (also with colors identifying the excitonic complexes) in time-resolved experiments correspond to the outcome of the microstate model with fitting values given in table 3, as explained below.

In CW excitation there is not a fixed temporal separation time between excitation events, which results in an almost continuous electron feeding of the QD and hence a clear predominance of the negative trion emission (under excitation at 830 nm). In contrast, exciton emission dominates under pulsed excitation. This behavior suggests that after a 'long period' without electron injection, the injected 'extra' electron escapes out of the QD, leaving it in its original empty situation. The non-radiative escape of the electron out of the QD at 10 K has no straightforward explanation. Direct or phonon-assisted tunneling is not probable without the existence of an accessible electronic level, like a neighbor QD. The access to WL states by thermal escape would be a possibility at low temperatures given the small energy difference from the QD ground state, especially in the case of confined holes.

4. Random population model

We adapt the RPM [2] to reproduce the capture and recombination dynamics of the different excitonic complexes in a shallow confined single QD with only one electron shell confined

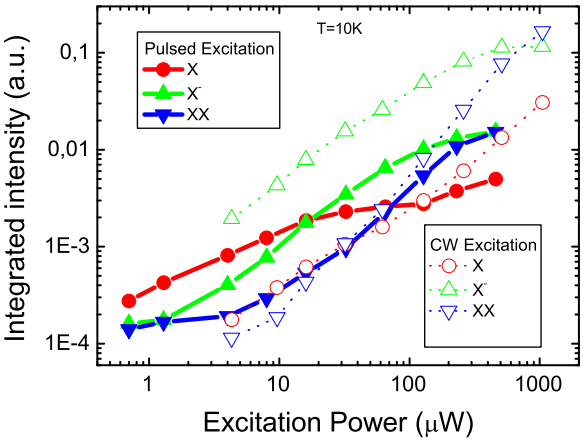

Figure 3. Experimental integrated intensity evolution exciting at 830 nm. Thick lines and solid symbols correspond to pulsed excitation, and dashed lines and hollow symbols to CW excitation.

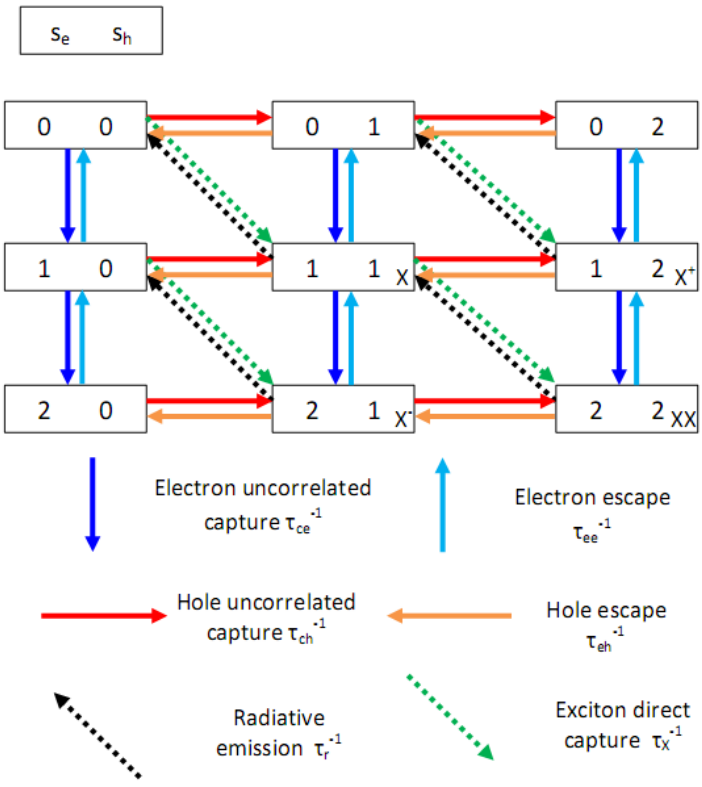

Figure 4. Diagram of the RPM model.

(s shell, s_e–s_h). Throughout this section we introduce the master equations for microstates (MEM) and check the validity of our assumptions by comparing the numerically simulated results and the experimental data.

Figure 4 presents a flow diagram of the MEM. Boxes represent the different charge configurations that a QD can present (microstate), the left number in the box specifies the number of electrons in the ground electron s shell (s_e), while the right number refers to

the number of holes in the ground hole s shell (s_h). Some microstates can be easily labeled as the conventional excitonic complexes: [1 1] ≡ X, [2 1] ≡ X^-, [1 2] ≡ X^+ and [2 2] ≡ XX, while [0 0] corresponds to an empty QD. Colored arrows refer to the possible mechanisms that effectively change the charge inside the QD: their result is always a microstate change.

MEM were developed to be applied on QD ensembles [2]. A time-resolved single QD spectra is the superposition of temporally differentiated events, as many as excitation cycles (integration time of the measurement per repetition rate of the excitation source). As a consequence, we can treat the optical properties of a single QD as generated by a 'temporal ensemble' of QDs. Every excitation cycle can be understood as an independent virtual QD event.

As an example, in the absence of excitation light the QD is empty, all virtual QDs of that 'temporal ensemble' are in the [0, 0] configuration, and the microstate populations (n_{ij} with $i, j = 0, 1, 2$) are

$$n_{00} = N_{\mathrm{QDs}}, n_{i,j} = 0 \quad \text{for all } i, j \neq 0, \tag{1}$$

where N_{QDs} is the number of QDs of our temporal ensemble, the number of excitation cycles. Imagine that only in one of the excitation cycles is an exciton captured. The virtual QD corresponding to that cycle would change from empty to occupied with one exciton and, as a consequence, the QD would change its microstate ($n_{00} \rightarrow n_{11}$). The total microstate population would evolve to

$$\begin{aligned} &n_{00} = N_{\mathrm{QDs}} - 1, n_{11} = 1, \\ &n_{01} = n_{02} = n_{10} = n_{12} = n_{20} = n_{21} = n_{22} = 0. \end{aligned} \tag{2}$$

The sum of all microstate populations remains always fixed at N_{QDs}. If we normalize the microstate population, that is, we set N_{QDs} to 1, the microstate population directly refers to the probability of finding a single QD in a particular microstate.

We will assume in this work that the QD is charged via the wetting layer (WL) in two different ways: exciton (or correlated e^- and h^+) capture and uncorrelated e^- and h^+ capture. In this way, two different WL level structures for both kinds of capture mechanisms are considered, as sketched in figure 5. In addition, an impurity level (ID) is included to account for the extra e^- injected when optical pumping is resonant with the ionized impurity levels.

The dynamics of the system is governed by the following system of differential equations:

$$\frac{\mathrm{d}n_{ij}}{\mathrm{d}t} = R_{ij}^{\mathrm{exc}}\mathrm{WL}_{\mathrm{exc}} + R_{ij}^{\mathrm{e}}\mathrm{WL}_{\mathrm{e}} + R_{ij}^{\mathrm{h}}\mathrm{WL}_{\mathrm{h}} + R_{ij}^{\mathrm{ee}} + R_{ij}^{\mathrm{eh}} + R_{ij}^{\mathrm{ID}}\mathrm{ID} + R_{ij}^{\mathrm{r}}, \tag{3}$$

$$\frac{\mathrm{dWL}_{\mathrm{exc}}}{\mathrm{d}t} = -\sum_{ij} E_{ij} R_{ij}^{\mathrm{exc}}\mathrm{WL}_{\mathrm{exc}} - \frac{\mathrm{WL}_{\mathrm{exc}}}{\tau_{\mathrm{W}}} + G_a, \tag{4}$$

$$\frac{\mathrm{dWL}_{\mathrm{e}}}{\mathrm{d}t} = -\sum_{ij} i R_{ij}^{\mathrm{e}}\mathrm{WL}_{\mathrm{e}} - \frac{\mathrm{WL}_{\mathrm{e}}}{\tau_{\mathrm{W}}} + G_b, \tag{5}$$

$$\frac{\mathrm{dWL}_{\mathrm{h}}}{\mathrm{d}t} = -\sum_{ij} j R_{ij}^{\mathrm{h}}\mathrm{WL}_{\mathrm{h}} - \frac{\mathrm{WL}_{\mathrm{h}}}{\tau_{\mathrm{W}}} + G_b, \tag{6}$$

$$\frac{\mathrm{dID}}{\mathrm{d}t} = -\sum_{ij} i R_{ij}^{\mathrm{ID}}\mathrm{ID} + G_c, \tag{7}$$

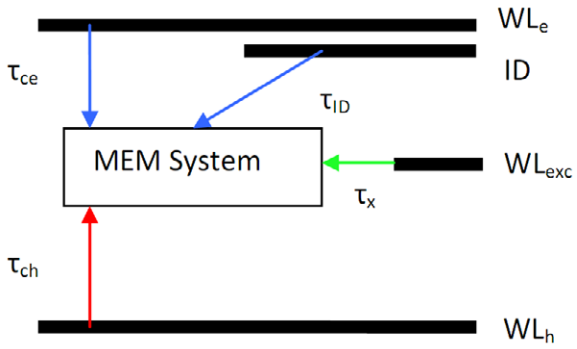

Figure 5. Interaction between the QD and its environment in the MEM model. WL_{exc} corresponds to the WL level for exciton-correlated capture, WL_e and WL_h to the WL levels for uncorrelated electron and hole captures, respectively, and ID is the source for extra electrons under resonant excitation to the impurity levels. The time constants τ_X, τ_{ce}, τ_{ch} and τ_{ID} are the QD capture times from WL_{exc}, WL_e, WL_h and ID levels, respectively.

where G_a, G_b and G_c are the excitation parameters to the levels WL_{exc}, WL_e and WL_h, and ID, respectively. WL_e and WL_h populations are symmetrically generated when exciting above the GaAs barrier. R_{ij} terms refer to the capture or escape processes that a single QD can undergo, as indicated in figure 4. Obviously these terms depend on the particular configuration of the QD. For example, an empty QD cannot lose an exciton via radiative decay. In the following subsections, we will describe and set these R_{ij} terms.

4.1. Exciton capture

Exciton capture (dashed green arrow in figure 4) is accounted for through the term R_{ij}^{exc} in equations (4) and (5). If one defines τ_X as the exciton capture time of an empty QD, the probability that a microstate loses population through exciton-correlated capture is

$$\left[R_{out}^{exc}\right]_{ij} = \frac{1}{2\tau_X}\left(\frac{I-i}{I} + \frac{J-j}{J}n_{ij}\right), \tag{8}$$

where I (J) is the maximum number of electrons (holes) that a QD can have. The probability that an empty QD captures an exciton is proportional to $\frac{1}{\tau_X}$ and the percentage of the virtual QDs on our temporal ensemble that are empty (n_{00}). In contrast, in a half full configuration, like [1,1], the probability is $\frac{1}{2\tau_X}n_{11}$; the factor $\frac{1}{2}$ comes from the fact that the QD in that configuration has only one free exciton level (s_e–s_h) instead of two. Probabilities for [0,1] and [1,0] are set to $\frac{3}{4\tau_X}n_{01}$ and $\frac{3}{4\tau_X}n_{10}$ following similar reasoning. For the rest of the microstates, the probability of losing population through a correlated exciton capture is zero (as an example, a QD with two e^- in s_e cannot capture an additional exciton, only an uncorrelated hole to complete one exciton). Remember that the sum of all microstate probabilities is always fixed: the decrease in population of one microstate results in an increase in the population of another microstate. It strictly means that the increment on n_{11}, n_{12}, n_{21} and n_{22} due to correlated exciton capture is due to the corresponding population decrease in n_{00}, n_{01}, n_{10} and n_{11}, respectively. In this way, we

can define the 'in' term like

$$\left[R_{\text{in}}^{\text{exc}}\right]_{ij} = \left[R_{\text{out}}^{\text{exc}}\right]_{(i-1)(j-1)}, \quad \text{for all } i,\, j \geqslant 1. \tag{9}$$

The effective change in the dot microstates induced by correlated exciton capture in our temporal ensemble will be

$$R_{ij}^{\text{exc}} = \left[R_{\text{in}}^{\text{exc}}\right]_{ij} - \left[R_{\text{out}}^{\text{exc}}\right]_{ij}. \tag{10}$$

The number of excitons actually captured from the WL_{exc} level can be calculated as a function of the microstate probability change, R^{exc}, by taking into account how many excitons can be found in a particular microstate (E_{ij}). It gives the term in equation (5):

$$\sum_{ij} E_{ij} R_{ij}^{\text{exc}} \text{WL}_{\text{exc}}, \tag{11}$$

where E_{ij}, the number of excitons in the microstate $[i, j]$, is equal to the minimum value between i and j.

4.2. Uncorrelated e^-–h^+ capture

The arguments given in the previous subsection can be also applied to uncorrelated e^-–h^+ capture (dark blue and red arrows in figure 4); free spaces in the receptor levels (s_e for e^- and s_h for h^+) determine the factors applied to every microstate:

$$\left[R_{\text{out}}^{\text{e}}\right]_{ij} = \frac{1}{\tau_{\text{ce}}} \frac{I - i}{I} n_{ij}, \tag{12}$$

$$\left[R_{\text{in}}^{\text{e}}\right]_{ij} = \left[R_{\text{out}}^{\text{e}}\right]_{(i-1)j} \qquad \text{for all } i \geqslant 1, \tag{13}$$

$$\left[R_{\text{out}}^{\text{h}}\right]_{ij} = \frac{1}{\tau_{\text{ch}}} \frac{J - j}{J} n_{ij}, \tag{14}$$

$$\left[R_{\text{in}}^{\text{h}}\right]_{ij} = \left[R_{\text{out}}^{\text{h}}\right]_{i(j-1)} \qquad \text{for all } j \geqslant 1. \tag{15}$$

The changes induced in the MEM system through these processes are

$$R_{ij}^{\text{e}} = \left[R_{\text{in}}^{\text{e}}\right]_{ij} - \left[R_{\text{out}}^{\text{e}}\right]_{ij}, \tag{16}$$

$$R_{ij}^{\text{h}} = \left[R_{\text{in}}^{\text{h}}\right]_{ij} - \left[R_{\text{out}}^{\text{h}}\right]_{ij}. \tag{17}$$

The changes in the feeding levels, WL_{e} and WL_{h}, that is, the number of captured e^- and h^+, are calculated (in equations (6) and (7)) as a function of R_{ij}^{e} and R_{ij}^{h} and the number of e^- (i) and h^+ (j) in microstates $[i, j]$.

4.3. Radiative decay

At cryogenic temperatures radiative recombination is the main mechanism for exciton losses. In our shallow QD, the biexciton lifetime (fitted by a single exponential decay to 0.65 ns) is half the exciton lifetime (1.27 ns) [9]. The radiative recombination probability is the same for every exciton (1.27 ns) because two recombination channels with equal probability are available in

the cascade process [5, 16]. However, not all QDs present the same behavior [17]. In our MEM approach, the radiative recombination term, proportional to the number of excitons in the QD, reads as

$$\left[R^{\mathrm{r}}_{\mathrm{out}}\right]_{ij} = \frac{1}{\tau_{\mathrm{r}}} E_{ij}, \tag{18}$$

$$\left[R^{\mathrm{r}}_{\mathrm{in}}\right]_{ij} = \left[R^{\mathrm{r}}_{\mathrm{out}}\right]_{(i-1)(j-1)} \qquad \text{for all } i,\, j \geqslant 1, \tag{19}$$

$$R^{\mathrm{r}}_{ij} = \left[R^{\mathrm{r}}_{\mathrm{in}}\right]_{ij} - \left[R^{r}_{\mathrm{out}}\right]_{ij}. \tag{20}$$

4.4. Injection of e^- under excitation resonant with impurities

Normally one could use an extra amount of e^- in the WL_e level to simulate the previously experimentally discussed effect of resonant pumping into the impurity energy levels. However, the distance between the excited impurities and the QD should play a role in the electron capture time. In order to differentiate both processes, uncorrelated e^- capture and impurity-mediated injection, we have included an extra level in our model that allows us to modify this capture time of electrons (τ_{ID}) and its delay (τ_{d}) independently, as experimentally observed. Further discussion on the delay time will be held in section 5. The matrix term $[R^{\mathrm{ID}}]_{ij}$ has the same functional terms as $[R^{\mathrm{e}}]_{ij}$, as both account for the same conceptual problem, uncorrelated e^- capture, but coming from different energetic levels and thus with different times. Now τ_{ID} applies to the transfer of e^- from impurities toward microstates.

4.5. Uncorrelated escape out of the quantum dot

We experimentally found evidence of the uncorrelated carrier escape out of QD for excitation resonant with the impurity levels, even if carrier escape is not expected at cryogenic temperatures due to the low phonon occupation and the small number of receptor levels for tunneling processes. A possible mechanism is the non-radiative transfer toward deep levels acting like electron traps. Uncorrelated hole escape could also be a feasible possibility if one thinks of the effect of a remaining positive charge in the QD long after excitation (it would strongly enhance X^- emission). This kind of effect needs a careful and quantitative study, which can be performed within the RPM framework. We include this mechanism in our model with R^{ee} for electron escape and R^{eh} for hole escape,

$$\left[R^{\mathrm{ee}}_{\mathrm{out}}\right]_{ij} = \frac{i}{\tau_{\mathrm{ee}}} n_{ij}, \tag{21}$$

$$\left[R^{\mathrm{ee}}_{\mathrm{in}}\right]_{ij} = \left[R^{\mathrm{ee}}_{\mathrm{out}}\right]_{(i+1)j}, \tag{22}$$

$$\left[R^{\mathrm{eh}}_{\mathrm{out}}\right]_{ij} = \frac{j}{\tau_{\mathrm{eh}}} n_{ij}, \tag{23}$$

$$\left[R^{\mathrm{eh}}_{\mathrm{in}}\right]_{ij} = \left[R^{\mathrm{ee}}_{\mathrm{out}}\right]_{i(j+1)}. \tag{24}$$

In contrast to uncorrelated e^-–h^+ escape, exciton escape as a whole should not have a consequence on the QD dynamics, because its effects would be equivalent to a reduction of the exciton capture. At low temperatures the escape of an exciton is even more improbable than the uncorrelated escape (the energy confining an exciton is the sum of the energies confining e^- and h^- plus the correction due to the binding energy). For the sake of simplicity we will not consider exciton escape in an explicit way.

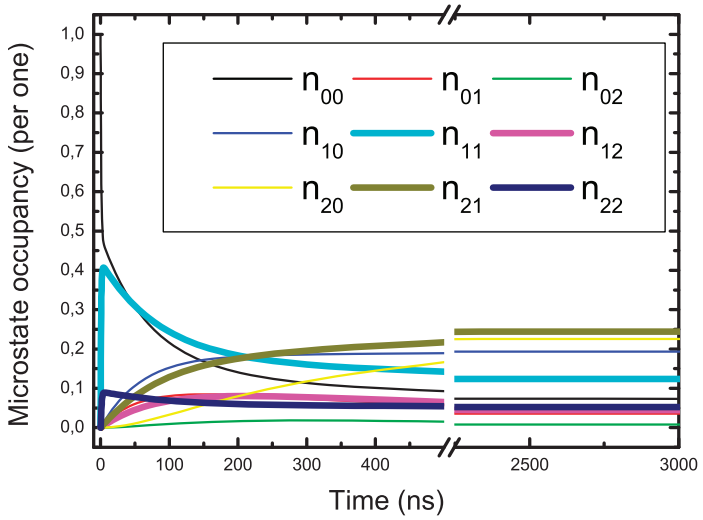

Figure 6. MEM typical output for CW excitation conditions. Thicker lines correspond to $X(n_{11})$, $X^+(n_{12})$, $X^-(n_{21})$, $XX(n_{22})$. Values used: $G_a = 0.1$ excitons ns^{-1}, $G_b = 0.02$ e$^-$–h$^+$ ns^{-1}, $G_c = 0$, $\tau_{ch} = 0.3$ ns, $\tau_{ce} = 0.7$ ns, $\tau_{eh} = 40$ ns, $\tau_{ee} = 12$ ns, $\tau_X = 5$ ps, $\tau_r = 1$ ns and $\tau_W = 0.45$ ns.

5. Simulation with the master equations for microstates model of CW and pulsed microphotoluminescence

Figure 6 shows the typical output of our MEM model described by equations (4)–(7) imposing CW excitation conditions. We solve the time-dependent partial derivative equations with a certain initial population distribution ($n_{00} = 1$ and 0 the other) under a given average excitation ($G_a = 0.1$ exciton ns^{-1}). The steady-state situation in the QD occupation is reached after several μs, as shown in figure 6. These occupation values are taken as the steady-state solution of the MEM model (those obtained in figures 7–9), instead of using a different numerical algorithm to solve equations (4)–(7) by setting the temporal partial derivatives to zero. In a similar way, imposing pulsed and periodic excitation ($G_{a,b,c} = G_{a,b,c}(t)$) we can use the same algorithm to calculate the temporal evolution of all excitonic populations (μTRPL transients), but we limit the calculation to 50 periods, as discussed below.

One of the main tools to identify the exciton and biexciton is the slope of their IPL power dependence. The slope of the exciton emission in a double logarithmic plot IPL versus excitation power should be close to 1, as the excitonic emission process is related one to one with e$^-$–h$^+$ or excitons created through optical injection. The slope for biexcitonic emission should be nearly 2 because the absorption of two excitons is needed in this case.

Figure 7 shows an MEM simulation as a function of the excitation power when only correlated exciton capture is considered. The slopes of X (0.99) and XX (1.99) nicely reproduce the ideal situation. A saturation plateau zone is achieved for a nominal excitation of 1 exciton ns^{-1} (1 ns is chosen as the exciton radiative lifetime in this simulation). The XX emission intensity grows at the expense of a reduction in the X emission intensity, leading to an XX probability close to one. There is no emission observed for X^- and X^+. The emission peaks X^- and X^+ appear when uncorrelated capture is considered, which is not the case of this example.

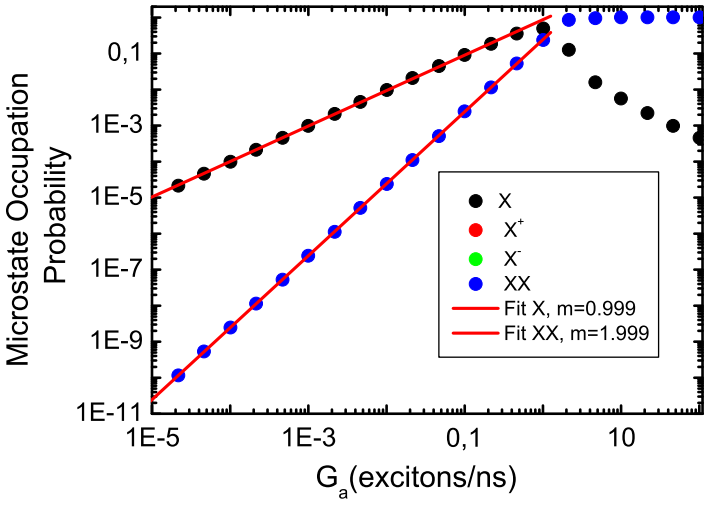

Figure 7. RPM simulation for only exciton capture and no escape mechanism.

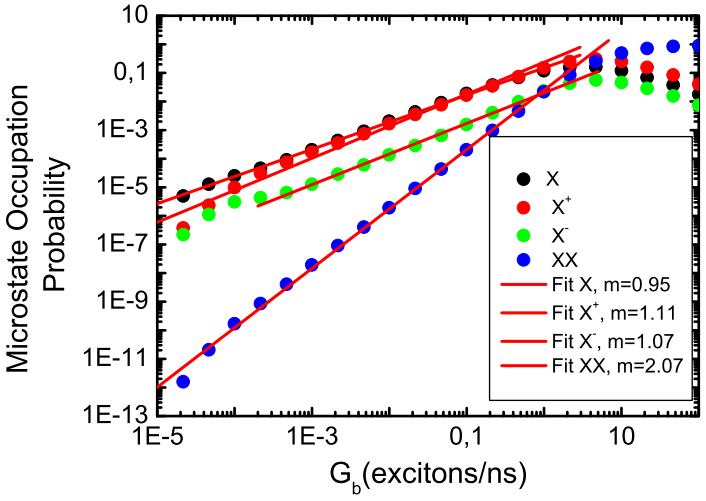

Figure 8. RPM simulation for only uncorrelated e^-–h^- capture and no escape mechanism.

The situation depicted in figure 8 is just the opposite of that illustrated in figure 7, i.e. only uncorrelated capture of e^- and h^+. In this case, we do not observe a linear dependence over the whole power range. When linear behavior is observed, the slopes for X and XX excitonic complexes present values slightly different from 1 and 2. Both charge trions (X^+ and X^-) appear with a linear slope close to 1. The simulation shows the X emission dominating at low and moderate powers (G_b below 0.1 exciton ns^{-1}), the residual e^- or h^+ tend to be compensated by the capture of their antagonist particle (and hence they contribute to enhance the X emission). X^+ trion dominates the emission between 0.2 and 3 excitons ns^{-1}, just before the XX growth (above 3 excitons ns^{-1}). In our experiments exciting above the GaAs barrier, we do not observe any trion emission dominating at any power. Because of that we will include both processes (correlated and uncorrelated capture) when simulating our CW experiments. To confront the MEM model with our experimental findings, we have developed a fitting routine for both CW and TRPL experiments.

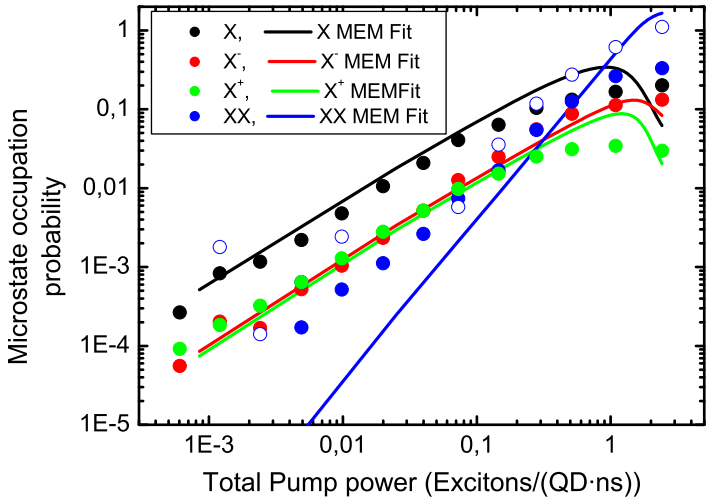

Figure 9. Integrated intensity evolution when exciting above the GaAs barrier. Solid lines correspond to fit experimental results for all excitonic complexes (solid circles) by using the fitting parameters in table 1. Hollow blue circles are calculated by subtracting the sum of X, X^- and X^+ intensities from the total experimental IPL (having contribution from biexcitonic charged excitonic complexes).

In all the fittings, some of the main parameters are chosen following the direct experimental measurements: $\tau_{WL} = 0.45$ ns, $\tau_r = 1$ ns. We have used $\tau_r = 1$ ns instead of $\tau_r = 1.27$ ns, the value obtained through a monoexponential fit, because we find better agreement in the TRPL fittings for all excitonic complexes with the reduced value (as shown below in figures 1 and 2). As τ_X, the capture time for excitons, we use a value taken from the literature $\tau_X = 5$ ps [18], well below our time resolution.

Figure 9 shows, for a different QD, the integrated intensity evolution when exciting in continuous wave above the GaAs barrier ($\lambda_{excitation} = 775$ nm). The axes in figure 9 also form part of the fitting result. Nice agreement is observed for the power dependence of all excitonic complexes, except the biexciton, for which the model overestimates the slope of the power dependence and the saturation value. The MEM result for XX fits better to the blue open circles that take into account both the existence of higher charged particles (XX^* extra peaks in high-power spectra) and a background lying under the excitonic emission peaks for the highest excitation powers. Better agreement could be obtained by adding to the model more excited microstates and/or screening effects with the environment, but it would increase the computational complexity of the fitting procedure as done in this work.

We find that a really small number of uncorrelated captures ($2.3 \times 10^{-3}\%$) has a dramatic impact on the appearance of charged excitons. Uncorrelated capture is really unlikely, only one out of every 43 000 excitons captured is captured in an uncorrelated way. In a pulsed experiment, with an average excitation of one exciton per cycle, we would need over 40 000 excitation cycles to capture an exciton in an uncorrelated way and that makes simulations of μTRPLs really difficult.

To simulate the time-resolved experiments, we use as excitation ($G_{a,b,c}(t)$) a delta function ($\delta(t)$), and we calculate the temporal evolution of the MEM system during an excitation cycle, a time τ_{rep} (the period of the pulsed laser used). The initial condition is

Table 1. CW fitting parameters corresponding to figure 9.

τ_{ch}	78 ps
τ_{ce}	20 ps
Percentage of uncorrelated captures	2.3×10^{-3}

Table 2. TRPL under non-resonant excitation to the impurities level fit parameters corresponding to figure 1.

τ_{ch}	1 ns
τ_{ce}	1.6 ns
Percentage of uncorrelated captures	7

an empty QD ($n_{0,0} = 1$) and WL. The results (the microstate populations) after τ_{rep} are used as new initial conditions for the new pulse arrival and so on. We introduce a delay (τ_d) in the impurity level excitation parameter ($G_c = G_c(t-\tau_d)$) to account for our experimental observations.

Typical acquisitions last several seconds, that is, millions of cycles, but we simulate our time-resolved experimental results (figure 1, excitation above the GaAs barrier) using only 50 cycles to allow a fit to the experiments. The best-fitting parameters listed in table 2 were obtained by minimizing the four situations depicted in figure 1. Obviously 50 pulses are not enough to reach a stable situation. In the CW fit (figure 9 and table 1), we found that for every 10 000 cycles only a few e^-–h^+ pairs are captured in an uncorrelated way. When we limit the number of cycles simulated, we artificially increase the percentage of uncorrelated captures. If we compare the electron and hole capture times to the ones obtained in the CW fitting procedure, even if they correspond to different QDs, we find a huge difference. Limiting the cycles in the simulations makes uncorrelated capture more probable (7–2.3×10^{-3}%) but the capture itself more unlikely (inverse of the electron and hole capture times).

In the case of resonant excitation with impurities, after checking that the real percentage of uncorrelated captures is smaller than the excess of injected e^- introduced when exciting resonance with the impurity levels, we neglect the process of uncorrelated e^-–h^+ capture. As previously discussed, μTRPL experimental data clearly point to the situation of empty QDs before the arrival of every pulse, in that case just one pulse simulation would be enough to describe them. For completeness reasons, we have simulated 50 pulses anyway in order to take into account any residual occupation accumulated between pulses (dark states, because we do not observe any luminescence 10 ns after the pulsed excitation).

The fitting procedure consists in the minimization of the global least squares of all four curves of figure 2; the four curves share τ_{ee}, τ_d, τ_{ID} and differ in the pumping parameters: the total pumping constant (ratios are fixed following the relation measured) and the percentage of that pumping that contributes to the impurity-related absorption (we present them in table 3). The simulation quantifies the delay between resonant capture into the QD and impurity-related capture (τ_d in table 3) and provides a lower capture rate through that channel ($\tau_{ID} \gg \tau_X$). The time that the extra electron remains in the QD ($\tau_{ee} = 10.8$ ns) is below the repetition period of the diode laser used (25 ns), compatible with the assumption of an empty QD before any excitation.

Table 3. Fitting parameters corresponding to TRPL under resonant excitation to the impurities level (figure 2).

τ_{ee}	10.8 ns
τ_d	0.23 ns
τ_{ID}	0.16 ns
Percentage of impurity absorption for I_0	28
Percentage of impurity absorption for $2 \times I_0$	38
Percentage of impurity absorption for $4 \times I_0$	67
Percentage of impurity absorption for $8 \times I_0$	86

We attribute that e^- escape time (τ_{ee}) to the time the system needs to recover the original situation after an impurity injects an extra electron into the QD. This escape time is surprisingly short for a QD held at cryogenic temperatures. Its origin should be connected through some non-radiative transfer toward deep levels (maybe electron traps), thermal promotion toward WL or both.

6. Conclusions

In conclusion, we have developed a random poulation model to account quantitatively for the appearance of charge excitons when exciting above the GaAs barrier as a result of low uncorrelated capture (about 10^{-3}% of the total captures, as estimated from CW experiments). The capture times for correlated carriers or excitons extracted with the model are below our experimental setup temporal resolution, while the uncorrelated capture times for e^- and h^+ depend on the local environment of the QD. We study the selective optical pumping phenomenon, a predominance of the negative trion observed when the optical excitation is resonant with a non-intentional impurity level, using time-resolved experiments. The μTRPL transients for the exciton emission appear before the negative trion emission, but its intensity exceeds completely that of the exciton after some hundreds of ps. We find a finite delay of about 230 ps (fitting result for τ_d in table 3) in the capture of the extra electrons. The origin of this delay is ascribed to transport from the impurity level. The study of the PL intensity under the different excitation conditions (pulsed and continuous waves) evidences uncorrelated electron escape with a escape time around 10 ns.

Acknowledgment

Thanks are given to 'Generalitat Valenciana' Project No. PROMETEO/2009/074 and the Spanish Ministry of Science through Project No. TEC2008-06756-C03-03.

References

[1] Warburton R, Schaflein C, Haft D, Bickel F, Lorke A, Karrai K, García J, Schoenfeld W and Petroff P 2000 *Nature* **405** 926

[2] Grundmann M and Bimberg D 1997 *Phys. Rev.* B **55** 9740

[3] Abbarchi M, Mastrandrea C, Kuroda T, Mano T, Vinattieri A, Sakoda K and Gurioli M 2009 *J. Appl. Phys.* **106** 053504
[4] Moskalenko E S, Karlsson K F, Holtz P O, Monemar B, Schoenfeld W V, García J M and Petroff P M 2002 *Phys. Rev.* B **66** 195332
[5] Chang W H, Chang H S, Chen W Y, Hsu T M, Hsieh T P, Chyi J I and Yeh N T 2005 *Phys. Rev.* B **72** 233302
[6] Moskalenko E S, Donchev V, Karlsson K F, Holtz P O, Monemar B, Schoenfeld W V, García J M and Petroff P M 2003 *Phys. Rev.* B **68** 155317
[7] Trevisi G, Seravalli L, Frigeri P and Franchi S 2009 *Nanotechnology* **20** 415607
[8] Muñoz-Matutano G, Alén B, Martínez-Pastor J, Seravalli L, Frigeri P and Franchi S 2008 *Nanotechnology* **19** 145711
[9] Muñoz-Matutano G, Gomis J, Alén B, Martínez-Pastor J, Seravalli L, Frigeri P and Franchi S 2008 *Physica* E **40** 2100
[10] Thompson R M, Stevenson R M, Shields A J, Farrer I, Lobo C J, Ritchie D A, Leadbeater M L and Pepper M 2001 *Phys. Rev.* B **64** 201302
[11] Warburton R J, Miller B T, Dürr C S, Bödefeld C, Karrai K, Kotthaus J P, Medeiros-Ribeiro G, Petroff P M and Huant S 1998 *Phys. Rev.* B **58** 16221
[12] Stevenson R M, Thompson R M, Shields A J, Farrer I, Kardynal B E, Ritchie D A and Pepper M 2002 *Phys. Rev.* B **66** 081302
[13] Alonso-González P, Alén B, Fuster D, González Y, González L and Martínez-Pastor J 2007 *Appl. Phys. Lett.* **91** 163104
[14] Moskalenko E S, Karlsson K F, Holtz P O, Monemar B, Schoenfeld W V, García J M and Petroff P M 2001 *Phys. Rev.* B **64** 085302
[15] Dekel E, Regelman D, Gershoni D, Ehrenfreund E, Schoenfeld W and Petroff P 2000 *Phys. Rev.* B **62** 11038
[16] Feucker M, Segui R, Rodt S, Hoffmann A and Bimberg D 2008 *Appl. Phys. Lett.* **92** 063116
[17] Bacher G, Weigand R, Seufert J, Kulakovskii V D, Gippius N A, Forchel A, Leonardi K and Hommel D 1999 *Phys. Rev. Lett.* **83** 4417–20
[18] Urayama J, Norris T B, Singh J and Bhattacharya P 2001 *Phys. Rev. Lett.* **86** 4930